

Supplementary file for

Rapid Disinfection of *E. coli* by Ternary BiVO₄/Ag/g-C₃N₄ Composite under Visible Light: Photocatalysis Mechanism and Performance Investigation in Authentic Sewage

Xiangkang Zeng ^a, Shenyu Lan ^a, Irene M.C. Lo ^{a, b, *}

^a Department of Civil and Environmental Engineering, The Hong Kong University of Science and Technology, Hong Kong, China

^b Institute for Advanced Study, The Hong Kong University of Science and Technology, Hong Kong, China.

* Corresponding author. Tel: +852 2358 7157, Fax: +852 2358 1534,

E-mail: cemclo@ust.hk (Prof. Irene M.C. Lo)

Text S1 *Chemicals and materials*

Melamine ($C_3H_6N_6$, 99.0%), bismuth chloride ($BiCl_3$, 98%), ammonium metavanadate (NH_4VO_3 , 99.0%), ethanolamine (C_2H_7NO , 99.0%), silver nitrate ($AgNO_3$, 99.8%), propidium iodide (PI, $C_{11}H_{34}I_2N_4$, 94%), 4', 6-diamidino-2-phenylindole (DAPI, $C_{16}H_{15}N_5 \cdot 2HCl$, 98%), terephthalic acid (TA, $C_8H_6O_4$, 98%) and glutaraldehyde solution (Grade I, 70% in H_2O) were purchased from Sigma-Aldrich. Methanol (CH_3OH , 99.9%) was obtained from Merck. Nitro blue tetrazolium chloride (NBT) was obtained from Invitrogen. All other chemicals, including sodium chloride ($NaCl$), ammonium oxalate ($C_2H_8N_2O_4 \cdot H_2O$), potassium dichromate ($K_2Cr_2O_7$), L-ascorbic acid, isopropanol, ethylenediaminetetraacetic acid (EDTA) disodium salt, iron (II) sulfate heptahydrate ($FeSO_4 \cdot 7H_2O$), hydrogen peroxide (H_2O_2), coumarin ($C_9H_6O_2$), sodium nitrate ($NaNO_3$), sodium sulphate (Na_2SO_4), potassium chloride (KCl), magnesium chloride hexahydrate ($MgCl_2 \cdot 6H_2O$) and calcium chloride dihydrate ($CaCl_2 \cdot 2H_2O$) were of analytical grade and used as received, without further purification. Suwannee River NOM (2R101N) was obtained from the international humic substances society. Luria-Bertani (LB) broth for the bacteria culture was purchased from Affymetrix. Throughout the assays, ultrapure deionized (DI) water was used ($18 M\Omega \cdot cm$, Cascada).

Text S2 *Characterizations of photocatalysts*

To detect the crystallite structure of the photocatalysts, powder X-ray diffraction (XRD) patterns of samples were measured in the range of 10–70 degree using a Philips PW1830 X-ray diffraction meter with Cu $K\alpha$ radiation ($\lambda = 1.5406 \text{ \AA}$). For

determining the light absorption ability and the optical properties of the as-prepared photocatalysts, UV-vis diffuse reflectance spectra (UV-DRS) of the photocatalysts were analyzed by a UV-Vis spectrophotometer (Lambda 950, Perkin Elmer, USA) with BaSO₄ as the internal reflectance standard. The morphologies of the photocatalysts were characterized by scanning electron microscopy (SEM, JEOL JSM-6390) and transmission electron microscopy (TEM, JEM-2010, JEOL). The specific surface area of the photocatalysts, after degassing at 150 °C for 3 h, were determined by N₂ adsorption-desorption based Brunauer – Emmett–Teller (BET) curves using a multi-station surface area analyzer at cryogenic temperature (NOVA-3200e, Quantachrome, USA). The functional groups of photocatalyst were analysed by Fourier-transform infrared (FTIR) spectrometry with the transmission mode (Vertex 70 Hyperion 1000, Bruker). To study the surface chemistry of the photocatalysts, X-ray photoelectron spectroscopy (XPS) analysis was undertaken using a PHI 5600 spectrometer (Physical Electronics) with a monochromated Al K α source at a power of 150 W. The photoluminescence (PL) spectra of photocatalyst suspension were obtained using a fluorescence spectrophotometer (F-4500, Hitachi), with excitation wavelength at 320 nm. For measuring the percentage of silver in the composite, 20 mg of the solid sample was dispersed in 10 mL of HNO₃ solution (5 vol%) and shaken for 24 h. The mixture was then filtered to remove the solid particles. The concentration of Ag ions in the solution was analyzed by a flame atomic absorption spectrophotometer (AAS, ZA3000 Hitachi).

Text S3 Analysis of reactive species

To determine which reactive species play the dominant role for photocatalytic *E. coli* inactivation by BiVO₄/Ag/g-C₃N₄, scavengers were added to the disinfection system to quench the corresponding active species under visible light irradiation: ammonium oxalate (0.5 mM) for h^+ elimination, potassium dichromate (0.5 mM) for e^- scavenging, Fe (II)-EDTA (0.5 mM) for H₂O₂ removal, L-ascorbic acid (0.5 mM) for superoxide radical ($\bullet\text{O}_2^-$) removal, and isopropanol(0.5 mM) for hydroxyl radical ($\bullet\text{OH}$). The applied concentration of scavenger was optimized to ensure the maximum scavenging effect but not to cause any inactivation of the bacterial cells ¹.

To further investigate the disinfection mechanism of the photocatalyst, the generation of reactive species in the photocatalytic process was measured in sterile saline solution containing the same amount of photocatalysts without *E. coli* cells. $\bullet\text{O}_2^-$ was measured with nitro blue tetrazolium (NBT, 0.025 mM) through measuring the absorbance at 259 nm by a UV-vis spectrophotometer as reported in our previous study ². Terephthalic acid (TA) at 0.5 mM in NaOH (2 mM) solution was used to detect the formation of $\bullet\text{OH}$ through measuring the spectrum on a fluorescence spectrophotometer at an excitation wavelength of 315 nm ³. To detect the concentration of H₂O₂ in the photocatalytic process, a fluorometric method was used with FeSO₄ and coumarin as the probes ⁴. During the photocatalytic process, 3 mL of the suspension was taken at certain irradiated times and filtered through a 0.22 μm filter (Millipore) to remove the photocatalysts. The filtrate was analyzed by a UV-Vis

Spectrophotometer (Lambda, PerkinElmer) or fluorescence spectrophotometer (F-4500, Hitachi) for absorbance or fluorescence measurement.

Text S4 *Electrochemical measurements*

Electrochemical characterizations were carried using a three-electrode cell on a CHI660D workstation (CH Instruments). To prepare the working electrodes, one milligram of the photocatalyst was added into 1 mL 0.5 % Nafion ethyl alcohol to form a slurry, sonicated for 30 min, and then dip-coated onto a 2 cm × 2 cm ITO glass electrode. Subsequently, the film electrodes were dried at 80 °C for 12 h. A platinum wire and an Ag/AgCl electrode were used as the counter electrode and the reference electrode, respectively. The transient photocurrent responses for the electrodes were measured under 1.0 V bias against the reference Ag/AgCl electrode. Electrochemical impedance spectra (EIS) were measured in the same electrolyte by applying a 5 mV alternative signal against the reference electrode over the frequency range of 1 MHz to 0.1 Hz. NaSO₄ aqueous solution (0.5 M) was used as the electrolyte, and a Xenon lamp (300 W, PLS-SXE300UV, Perfect Light) with a 420 nm cut-off filter was used as the visible light source throughout the experiment.

Text S5 *Effects of sewage components on photocatalytic disinfection*

The effects of sewage components (suspended solids, dissolved NOM and inorganic ions) on photocatalytic disinfection were investigated in saline solution through mimicking the sewage component individually. To mimic the suspended solids (8.8 mg/L, **Table S1**) in sewage, 50 mL of the sewage sample was filtrated

through a membrane (Pall Supor[®], 0.45 μm , 47 mm) and the collected solids were re-suspended in 50 mL *E. coli* (3×10^6 CFU/mL) saline suspension. As the content of total organic carbon (TOC) in sewage was 11.4 ± 1.5 mg/L (**Table S1**), to simulate the NOM, the commercial Suwannee River NOM (10 mg/L) was added to the *E. coli* saline suspension. To mimic inorganic ions in the sewage (**Table S1**), a mixed salts stock solution (200 mg/L NaNO₃, 1,050 mg/L Na₂SO₄, 1,490 mg/L KCl, 9,390 mg/L MgCl₂·6H₂O, and 6,690 mg/L CaCl₂·2H₂O; total inorganic ionic strength of this stock was calculated to be 286.05 mM) was prepared. One milliliter of the above stock solution was then added to 49 mL *E. coli* saline suspension to mimic the mixture of inorganic ions in the sewage.

The photocatalytic degradation of NOM in sewage was determined by the analysis of the TOC using a TOC analyzer (TOC-L, Shimadzu). The changes of NOM in the sewage during the photocatalytic process were also analyzed by excitation-emission matrix (EEM) fluorescence spectroscopy. During the photocatalytic process in the sewage, 3 mL of the suspension was taken at a certain irradiated time and centrifuged (10000 rpm for 10 min) to remove the photocatalysts, and the supernatants were used for EEM fluorescence spectroscopy. Fluorescence spectra were recorded with a fluorescence spectrophotometer (F-4500, Hitachi) using a 700W Xe lamp. To acquire the EEM spectra, the excitation wavelengths were increased from 230 to 400 nm at 10 nm intervals; for each excitation wavelength, the emission was recorded from 250 to 500 nm at 1 nm intervals.

Text S6. Electrochemical characterization of photocatalysts

In photocatalysis, the generation of reactive species is closely associated with the lifetime and separation of e^-h^+ pairs. To investigate the charge carrier separation efficiency of photocatalysts, electrochemical characterizations were conducted. As illustrated in **Fig.S14a**, the photocurrent density of the BiVO_4 or $g\text{-C}_3\text{N}_4$ is quite small, indicating the rapid recombination of the photo-induced charge carrier in the individual photocatalyst. Coupling BiVO_4 with $g\text{-C}_3\text{N}_4$ improved the separation of the charges, resulting in an enhanced photocurrent density. When Ag nanoparticles were introduced, $\text{BiVO}_4/\text{Ag}/g\text{-C}_3\text{N}_4$ had a higher photocurrent density in comparison with that in the $\text{BiVO}_4/g\text{-C}_3\text{N}_4$ counterpart. These results indicated that Ag nanoparticles could promote the separation of charge carriers between BiVO_4 and $g\text{-C}_3\text{N}_4$. To further investigate the charge transfer process, electrochemical impedance spectra (EIS) Nyquist plots of $\text{BiVO}_4/\text{Ag}/g\text{-C}_3\text{N}_4$ and $\text{BiVO}_4/g\text{-C}_3\text{N}_4$ were obtained. **Fig.S14b** shows that the semicircle size of the $\text{BiVO}_4/\text{Ag}/g\text{-C}_3\text{N}_4$ electrode is smaller than that of the $\text{BiVO}_4/g\text{-C}_3\text{N}_4$ electrode, indicating the lower resistance for electron transfer in $\text{BiVO}_4/\text{Ag}/g\text{-C}_3\text{N}_4$ ⁵. Furthermore, the lifetime (τ) of the injected electrons was analyzed using the Bode-phase of the two photocatalyst electrodes. As illustrated in **Fig.S14c**, the $\text{BiVO}_4/g\text{-C}_3\text{N}_4$ electrode shows a peak at a frequency of 562,500 Hz. The peak was shifted to a lower frequency (382,800 Hz) in the $\text{BiVO}_4/\text{Ag}/g\text{-C}_3\text{N}_4$ electrode. The frequency is closely related to the lifetime (τ) of the injected electrons as follows: $\tau \approx 1/(2\pi f)$ ⁶. From the equation, the electron lifetime of the $\text{BiVO}_4/\text{Ag}/g\text{-C}_3\text{N}_4$ (0.42 μs) electrode was estimated to be 1.5 times longer than that

of the BiVO₄/g-C₃N₄ (0.28 μs) electrode. The charge separation was further investigated by photoluminescence (PL) spectra of the BiVO₄/g-C₃N₄ and BiVO₄/Ag/g-C₃N₄ suspensions. As illustrated in **Fig.S14d**, an obvious peak, which is due to the recombination of e⁻-h⁺ in photocatalysis, appears in the PL spectrum of the BiVO₄/g-C₃N₄ composite. When Ag nanoparticles were deposited onto BiVO₄, the intensity of the peak in the PL spectrum was significantly decreased, indicating the recombination of e⁻-h⁺ in BiVO₄/Ag/g-C₃N₄ composite was inhibited. Therefore, using Ag nanoparticles as a bridge at the interface between the BiVO₄ and g-C₃N₄ could be an effective way to separate the charge carrier, thus promoting the generation of reactive species.

Text S7. CB and VB band position of photocatalyst

For a semiconductor at the point of zero charges, the edge potential of the conduction band (CB) and valence band (VB) can be estimated from **equation 1 and 2**^{7,8} as follows:

$$E_{CB} = X - E_e + 0.5 E_g \quad (1)$$

$$E_{VB} = E_{CB} + E_g$$

(2)

Here E_{CB} and E_{VB} are the CB edge potential and VB edge potential, respectively, X is the electronegativity of the semiconductor; E_e is the energy of the free electrons on the hydrogen scale (ca. 4.5 eV vs NHE) and E_g is the band gap energy of the semiconductor. According to previous studies, the electronegativity of BiVO₄ and

g-C₃N₄ were calculated to be 6.04 eV⁹ and 4.64 eV¹⁰, respectively. From the above equations, the CB and VB potentials of BiVO₄ were calculated to be +0.31 eV vs NHE and +2.77 eV vs NHE, respectively. Meanwhile, for g-C₃N₄, its CB and VB potentials were calculated to be -1.23 eV vs NHE and +1.51 eV vs NHE, respectively.

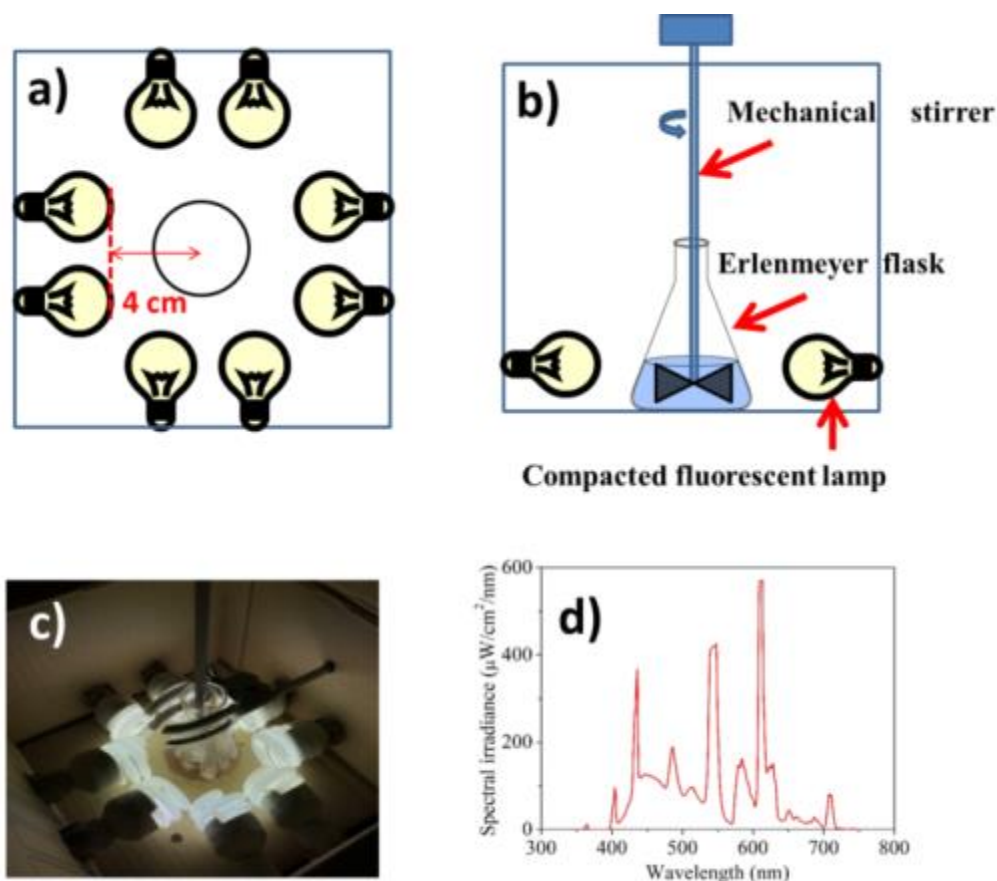


Fig.S1 Photocatalytic reactor set-up: (a) Schematic diagram of the photocatalytic reactor (top view); (b) Schematic diagram of the photocatalytic reactor (front view); (c) The picture of the photocatalytic reactor; (d) The spectral irradiance spectrum measured inside the Erlenmeyer flask (at the center) surrounded by eight compacted fluorescent (CFL) lamps(Philips Mini 8W E14 Cool Daylight, Netherlands). As illustrated in Fig. d, the major peaks in the spectrum belong to the visible-light region (400-700 nm) and the UV-component (i.e., peaks at wavelength<400 nm) was negligible. Hence the setup served as a good visible-light source. The spectral irradiance (E) in the center of the reactor was measured using a spectroradiometer. Subsequently, the integrated irradiance from 300 nm to 800 nm was calculated to be 330 W/m^2 , which was defined as the spectral irradiance (E) integrated over the wavelength interval from 300 nm to 800 nm from the equation: $E_{300-800} = \int_{300}^{800} E_{\lambda} d\lambda$

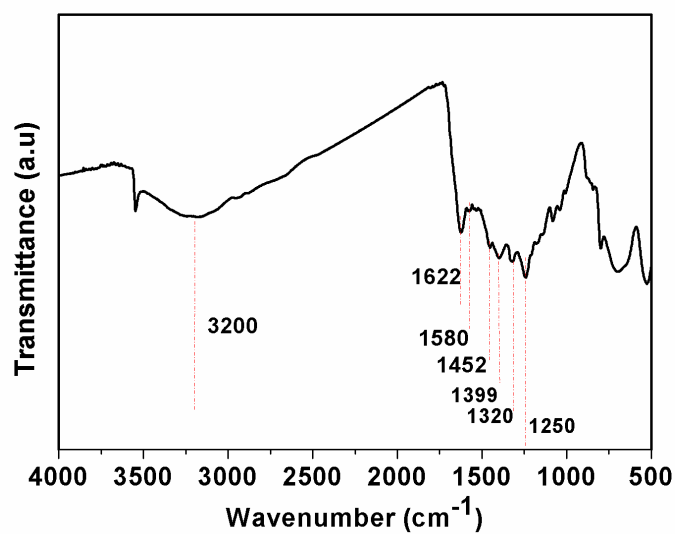


Fig.S2. FTIR spectrum of BiVO₄/Ag/g-C₃N₄

The absorption bands at 1622, 1580, 1452, 1399, 1320, and 1250 cm⁻¹ belonged to the typical stretching vibration modes of the g-C₃N₄ heterocycles¹¹. The broad adsorption band centered at 3200 cm⁻¹ is attributed to the N-H stretching vibration¹¹.

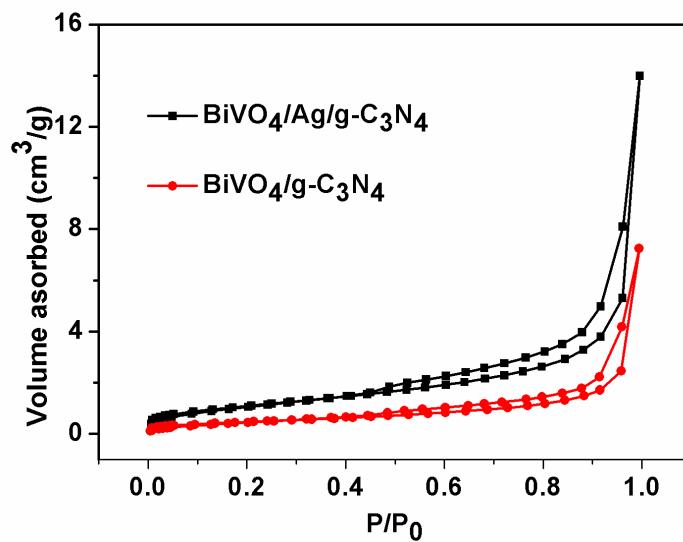


Fig. S3. Nitrogen sorption isotherm of BiVO₄/Ag/g-C₃N₄ and BiVO₄/g-C₃N₄

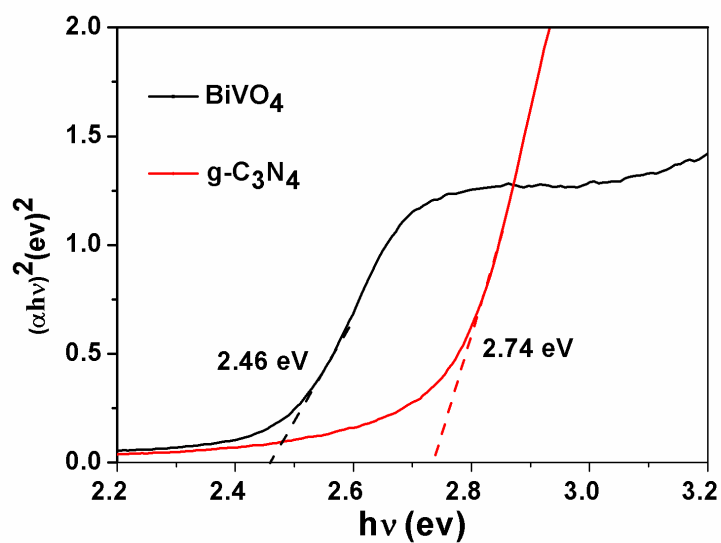


Fig.S4 The optical bandgaps of pure BiVO₄ and g-C₃N₄ calculated from the Tauc's plot using Kubelka-Munk equation

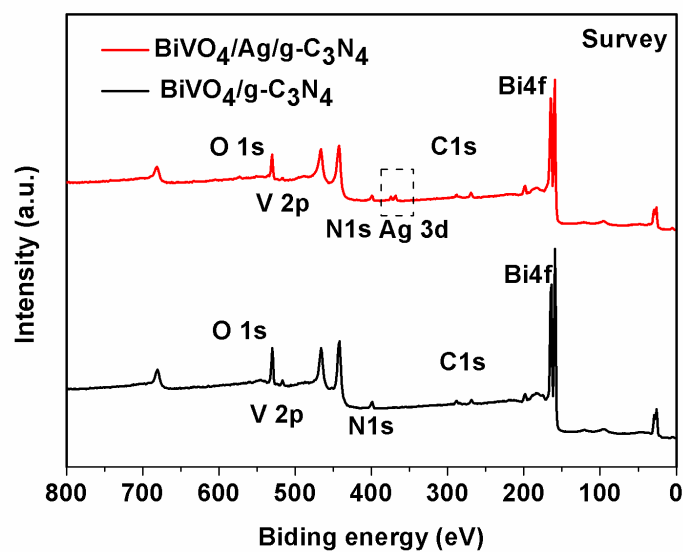


Fig.S5 XPS survey spectra of the BiVO₄/Ag/g-C₃N₄ and BiVO₄ /g-C₃N₄ composites.

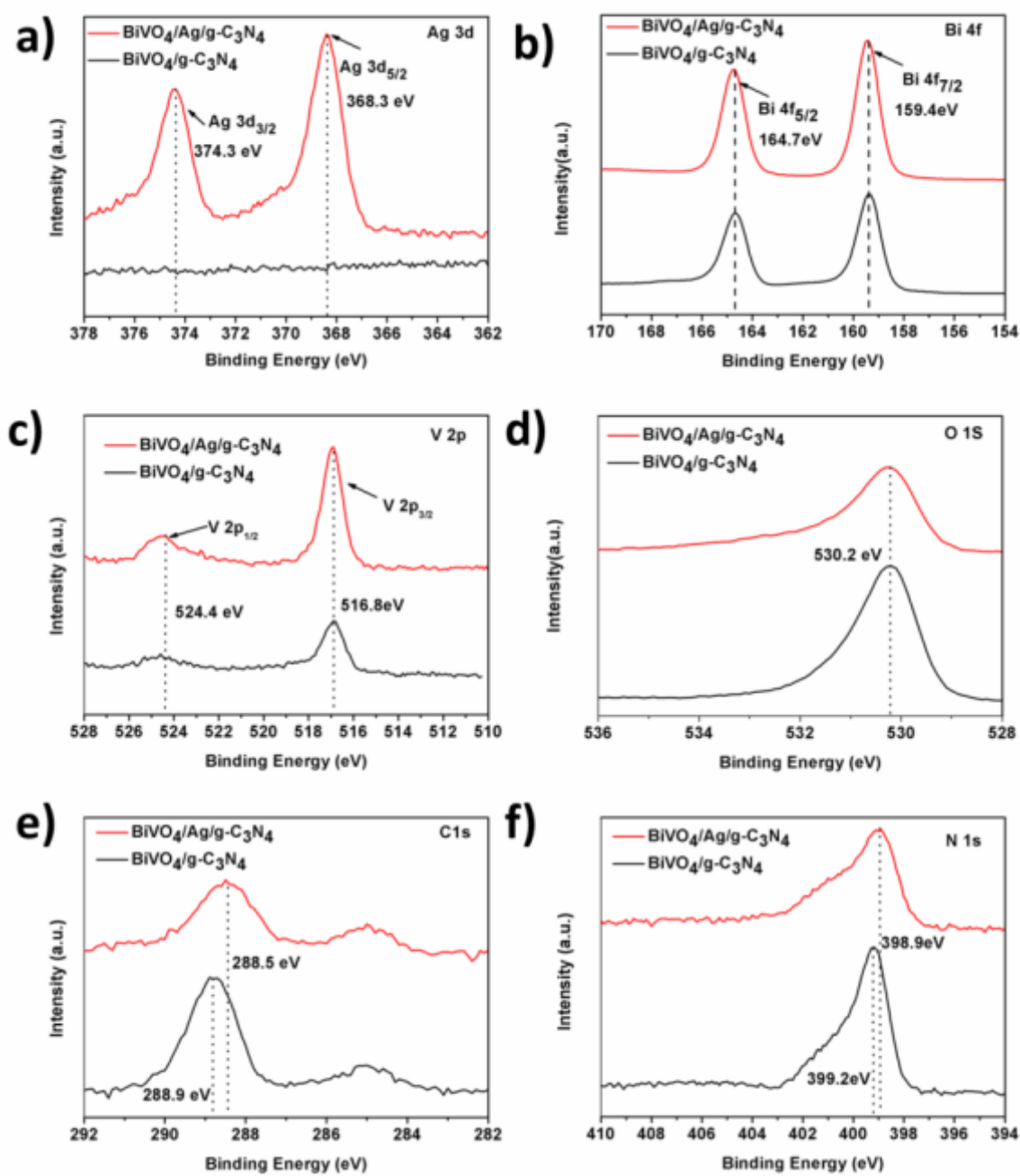


Fig.S6 High-resolution XPS spectra of the $\text{BiVO}_4/\text{g-C}_3\text{N}_4$ and $\text{BiVO}_4/\text{Ag}/\text{g-C}_3\text{N}_4$ composites: (a) Ag 3d, (b) Bi 4f, (c) V 2p, (d) O 1s, (e) C1s and (f) N1s

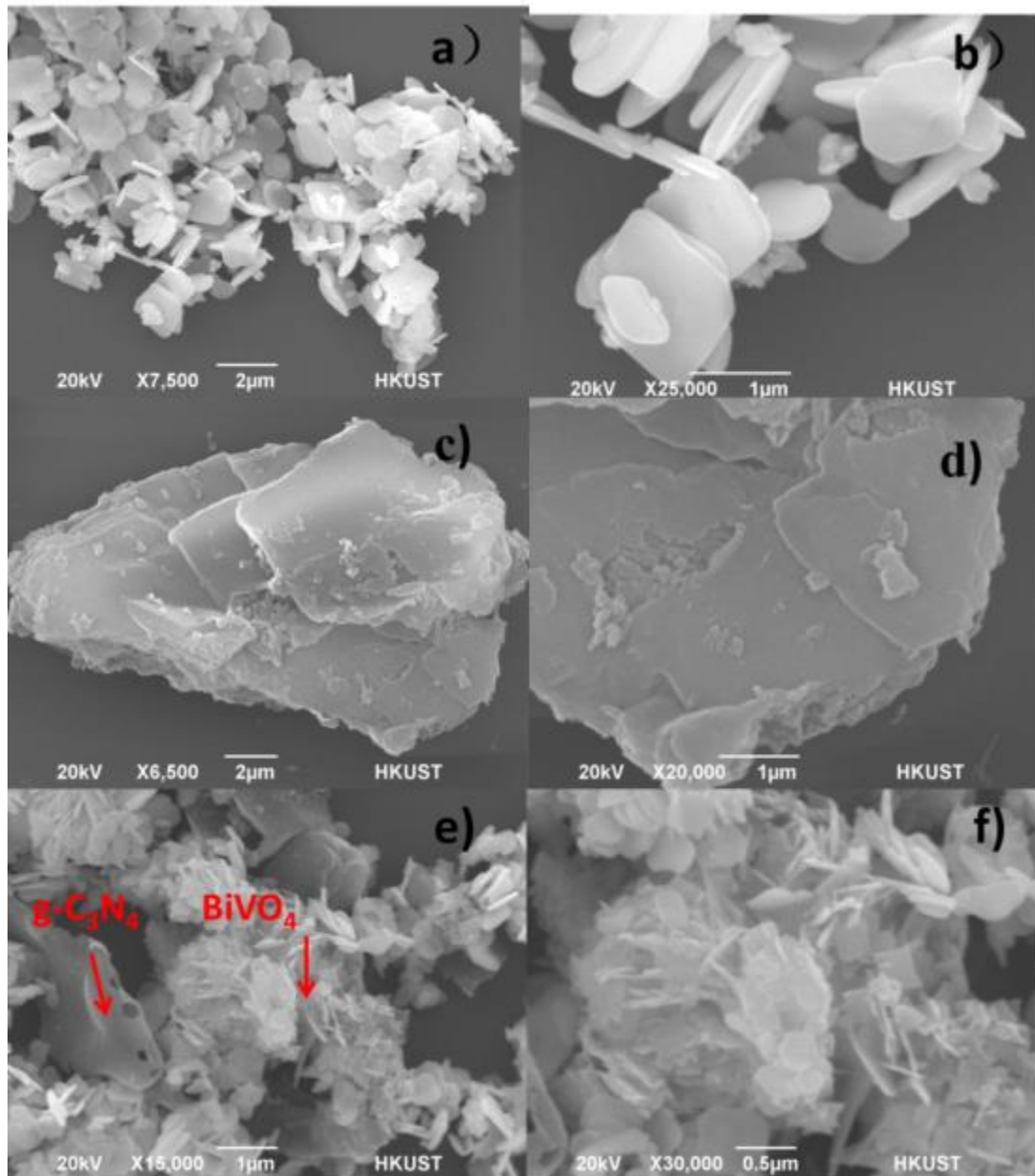


Fig.S7 (a-b) SEM images of BiVO₄, (c-d) bulk g-C₃N₄ and (e-f) BiVO₄ /g-C₃N₄ composite

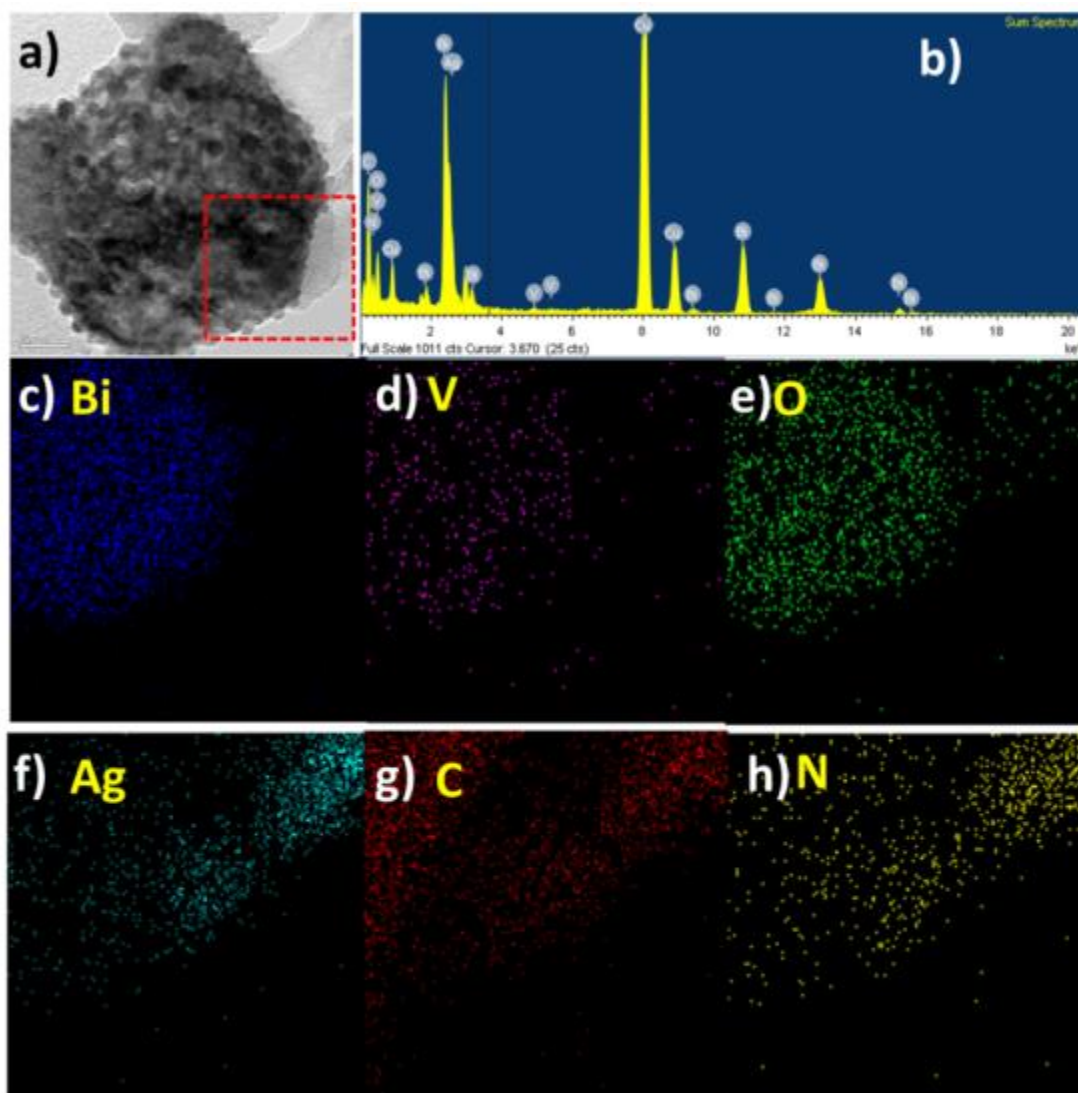


Fig.S8 TEM energy-dispersive X-ray (TEM-EDX) spectroscopy elemental mapping images of the $\text{BiVO}_4/\text{Ag}/\text{g-C}_3\text{N}_4$ composite: (a) TEM image of $\text{BiVO}_4/\text{Ag}/\text{g-C}_3\text{N}_4$ composite, the red square area shows the selected EDX mapping area; (b) EDX spectrum of the $\text{BiVO}_4/\text{Ag}/\text{g-C}_3\text{N}_4$ shows the elements in the composite; The corresponding EDX elemental mapping for (c) Bi, (d) V, (e) O, (f) Ag, (g) C, and (h) N.

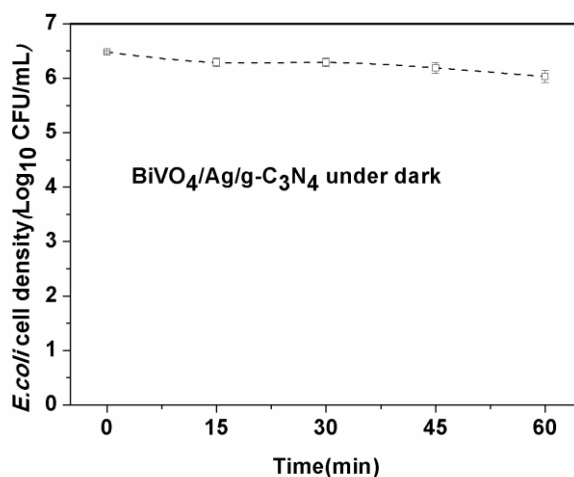


Fig.S9 The inactivation of *E. coli* cells by $\text{BiVO}_4/\text{Ag}/\text{g-C}_3\text{N}_4$ composite under dark condition; the dosage of photocatalyst was 0.25 g/L

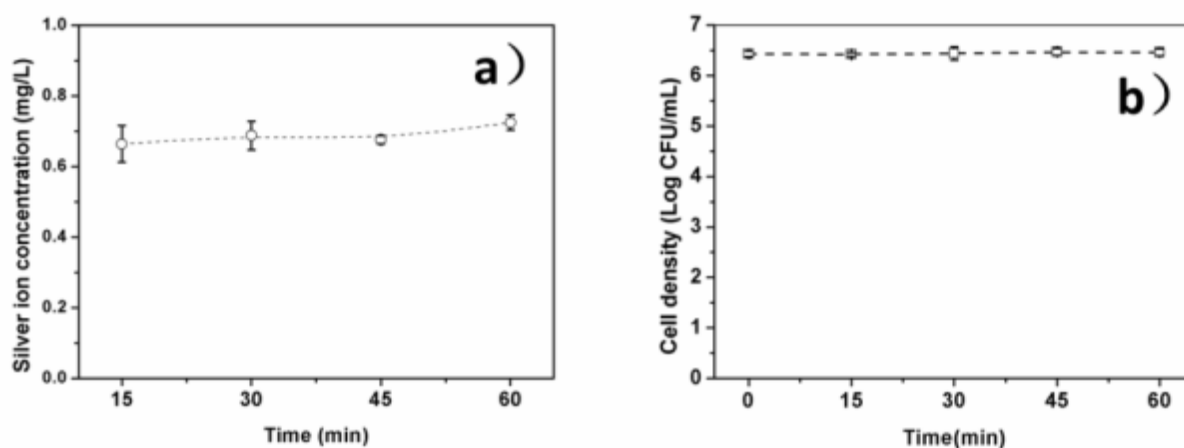


Fig.S10 (a) Ag ions leaking from the $\text{BiVO}_4/\text{Ag}/\text{g-C}_3\text{N}_4$ composite (0.25 g/L) in 0.9 w% NaCl solution under visible light irradiation; (b) Effect of the Ag ions (0.7 mg/L) on the viability of *E. coli* cells. The concentration of Ag ions in the solution was analyzed by a flame atomic absorption spectrophotometer (ZA3000, Hitachi)

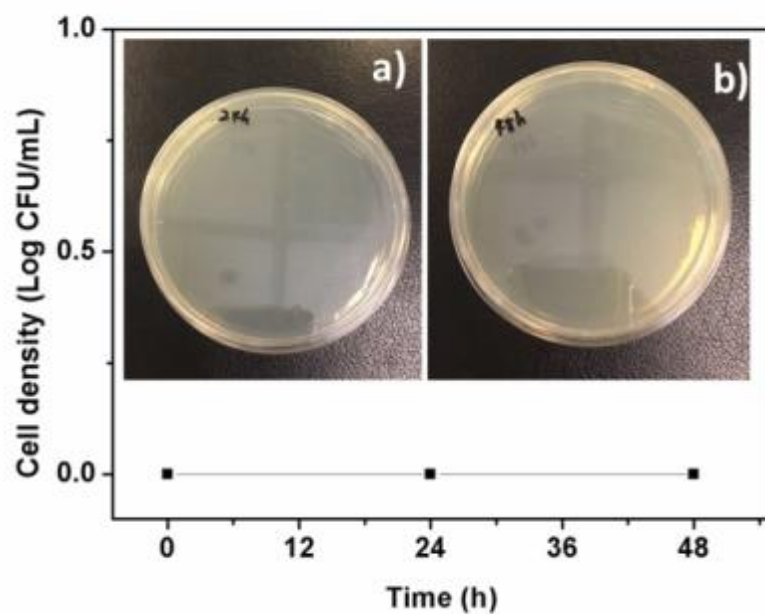


Fig. S11 Regrowth test of *E. coli* cells with a recovery period of 24 h and 48 h after photocatalytic disinfection by $\text{BiVO}_4/\text{Ag}/\text{g-C}_3\text{N}_4$; the inset pictures show no *E. coli* colony formed after a recovery period of (a) 24 h and (b) 48 h

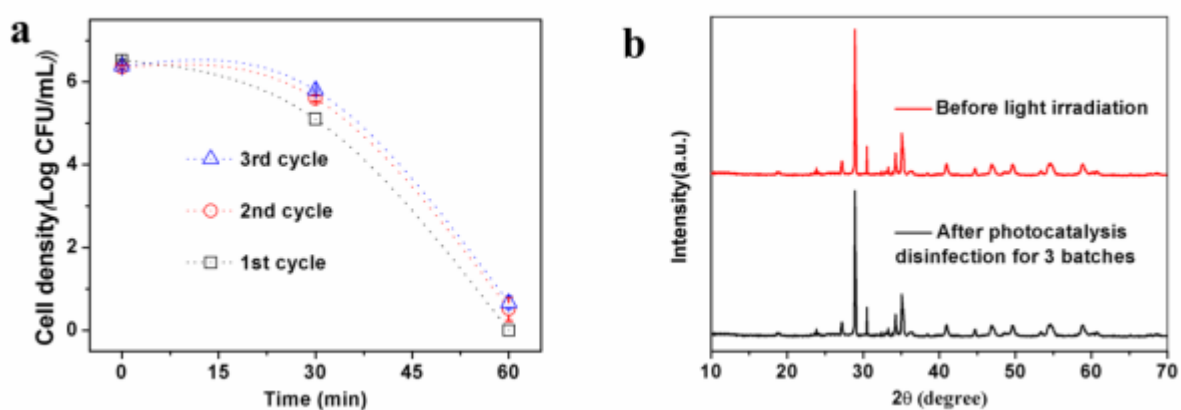


Fig. S12 (a) Recycle disinfection performance of the $\text{BiVO}_4/\text{Ag}/\text{g-C}_3\text{N}_4$ under visible light and (b) XRD pattern of $\text{BiVO}_4/\text{Ag}/\text{g-C}_3\text{N}_4$ before and after disinfection.

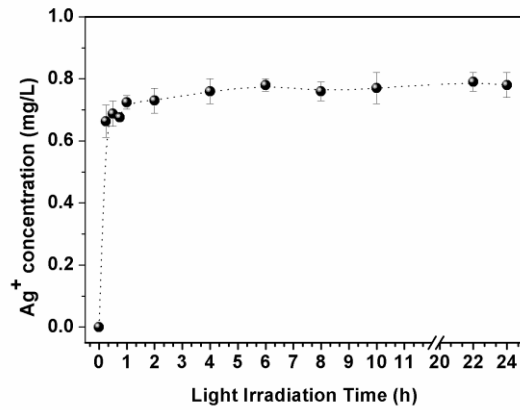


Fig. S13 Leaked Ag ions from the BiVO₄/Ag/g-C₃N₄ composite (0.25 g/L) in 0.9 w% NaCl solution under visible light irradiation

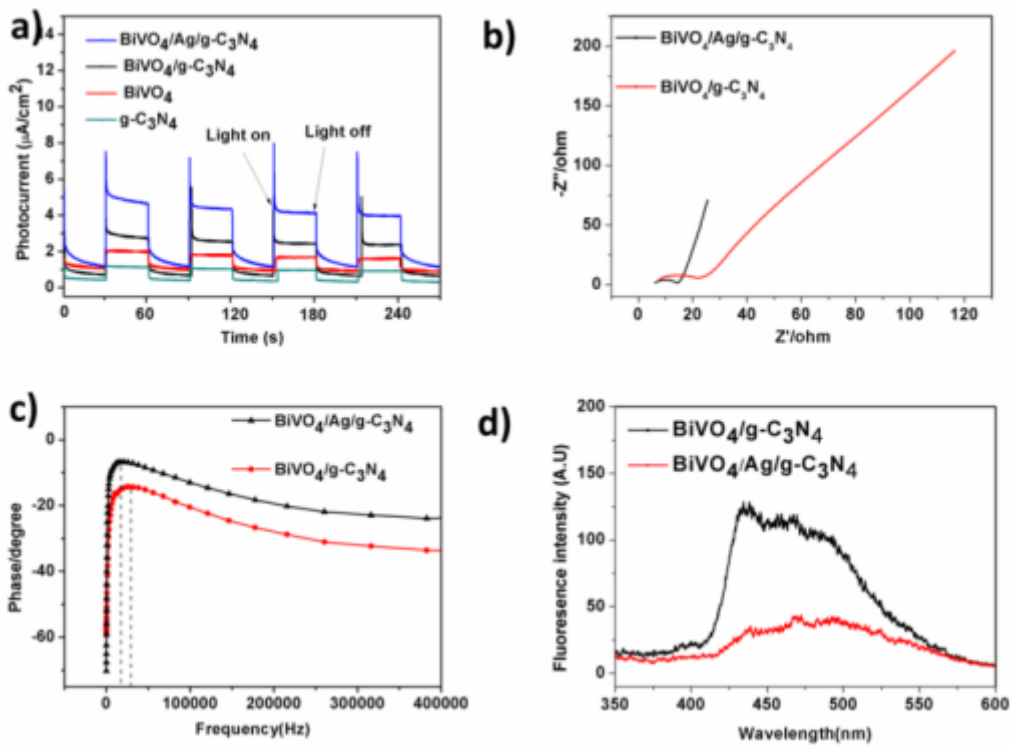


Fig. S14 (a) Photocurrent response (I-t) curve of g-C₃N₄, BiVO₄, BiVO₄/g-C₃N₄ and BiVO₄/Ag/g-C₃N₄; (b) EIS Nyquist plots of the BiVO₄/g-C₃N₄ and BiVO₄/Ag/g-C₃N₄ electrodes under visible light irradiation; (c) The Bode-phase of the BiVO₄/g-C₃N₄ and BiVO₄/Ag/g-C₃N₄ electrodes under visible light irradiation; (d)

Photoluminescence (PL) spectra of $\text{BiVO}_4/\text{g-C}_3\text{N}_4$ and $\text{BiVO}_4/\text{Ag/g-C}_3\text{N}_4$ suspensions; the concentration of photocatalyst was 1 g/L, and exciting wavelength was 320nm.

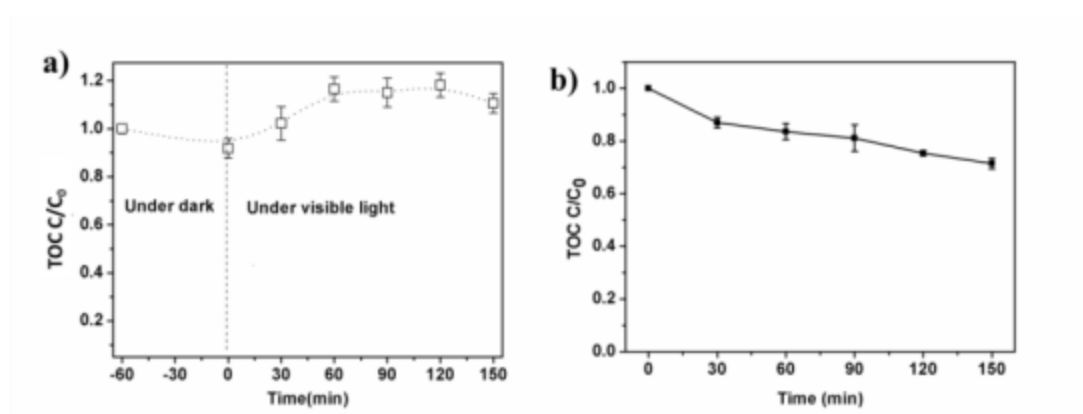


Fig.S15 Changes of total organic carbon (TOC) in (a) sewage and (b) commercial NOM solution (10 mg/L) during photocatalytic disinfection process by $\text{BiVO}_4/\text{Ag/g-C}_3\text{N}_4$ under visible light irradiation; the dosage of photocatalyst was 0.25 g/L

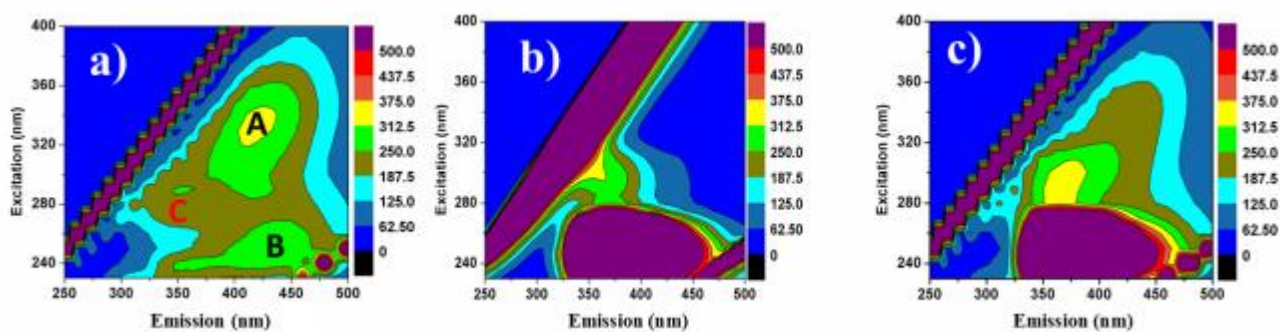


Fig.S16 (a) Fluorescence EEM spectrum of secondary treated effluent from Sai Kung STWs; The A-C peaks were humic-like substances, fulvic-like substances, and protein-like substance, respectively; (b) Fluorescence EEM spectrum of supernatant of photocatalyst suspension after centrifugation, which shows a big fluorescent area (purple) due to the remaining photocatalyst in the supernatant; (c) Fluorescence EEM spectrum of the supernatant of sewage and photocatalyst suspension after centrifugation, it showed the overlap of figure a and b.

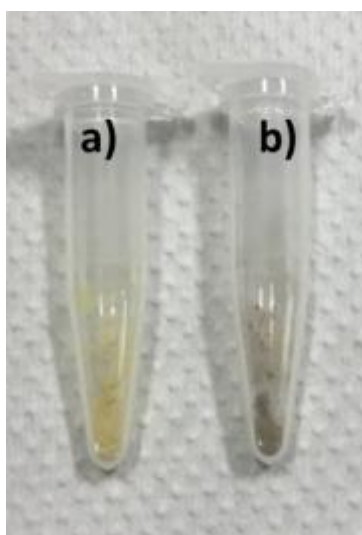


Fig.S17 Photos of $\text{BiVO}_4/\text{Ag}/\text{g-C}_3\text{N}_4$ after photocatalytic disinfection reaction in 0.9% NaCl solution (a) and actual sewage (b) under visible light for 60 min.

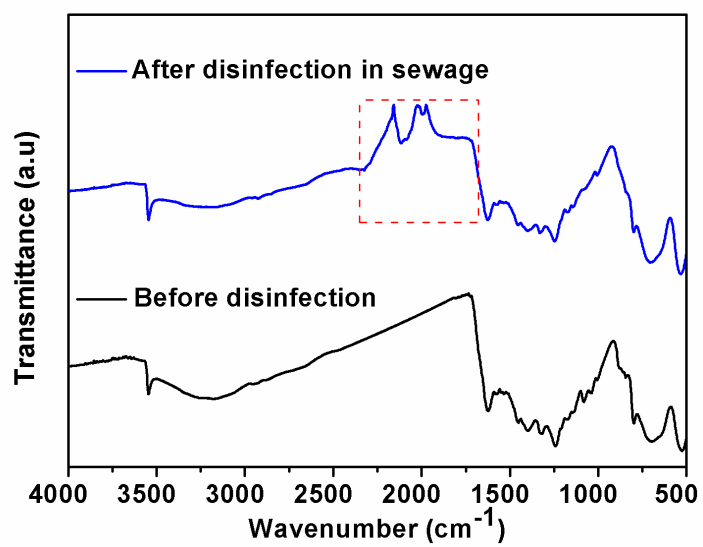


Fig.S18 FTIR spectra of BiVO₄/Ag/g-C₃N₄ before and after disinfection in sewage

Table S1. The physicochemical properties of secondary treated effluent from a local sewage treatment works

Parameter	Value*
pH	6.9 ± 0.0
Total suspended solids (mg/L)	8.5±0.3
TOC (mg/L)	11.4 ± 1.5
TN (mg/L)	2.41 ± 0.35
Cl⁻ (mg/L)	171.2 ± 10.7
NO₃⁻-N (mg/L)	2.91 ± 0.11
SO₄²⁻-S (mg/L)	14.20 ± 0.76
Ca²⁺ (mg/L)	36.4 ± 0.1
K⁺ (mg/L)	17.9 ± 0.1
Mg²⁺ (mg/L)	22.2 ± 0.0
Bacteria density (CFU/100mL)	450,000 ± 50,000

Please note that the sewage sample is a non-saline sewage and its salinity level is low compared with the wastewater receiving from seawater for toilet flushing in Hong Kong. The pH of sewage was measured by a pH meter (inoLab, WTW Series pH 720) at 25 °C; To measure the total suspended solids, 200 mL sewage was filtrated by a 0.45µm membrane and the solids on the membrane was dried at 105 °C and weighed; Total organic carbon (TOC) and total nitrogen (TN) in sewage were determined by a total organic carbon analyzer equipped with a TN unit (TOC-L, TNM-L, Shimadzu, Japan); The concentration of anions was measured using an ion chromatograph (HIC-20A super, Shimadzu, Japan) equipped with a conductivity detector and an IC-SA2 analytical column (Shim-pack IC-SA2, Shimadzu, Japan); The concentration of cations in sewage was measured by an Inductively Coupled Plasma-Optical Emission Spectrometer (Varian, Australia). To determine the bacterial density, 0.1 ml of diluted sewage (diluted 10 times with saline solution) was spread onto LB agar plates and incubated at 37 °C for 18 h to form viable colony units. All the colonies formed on the LB agar plates were regards as bacteria and counted for bacteria density measurement.

Table S2. Surface area of BiVO₄/Ag/g-C₃N₄ and BiVO₄/g-C₃N₄

Photocatalysts	BiVO ₄ /Ag/g-C ₃ N ₄	BiVO ₄ /g-C ₃ N ₄
BET Surface area (m ² /g)	18.168	13.960

Table S3. BiVO₄ and g-C₃N₄ based photocatalysts for visible-light-driven inactivation of bacteria

Photocatalysts	Catalyst dosage	Light source	Target bacteria	Disinfection performance	Ref.
BiVO ₄ nanotube	0.2 g/L	300W Xe lamp with a 400 nm cutoff filter	<i>E. coli</i> K-12	5.3 log in 5h	¹
g-C ₃ N ₄	1 g/L	300W Xe lamp with a 400 nm cutoff filter	<i>E. coli</i> K-12	6.4 log in 4h	12
g-C ₃ N ₄ (atomic single layer)	0.1 g/L	500W Xe lamp with a 400 nm cutoff filter	<i>E. coli</i>	7.3 log in 4h	13
Porous g-C ₃ N ₄	0.4 g/L	500W Xe lamp with a 400 nm cutoff filter	<i>E. coli</i>	6.68 log in 4h	14
Ag/g-C ₃ N ₄	0.1 g/L	300W Xe lamp with a 400 nm cutoff filter	<i>E. coli</i>	7 log in 1.5 h	15
Ag/g-C ₃ N ₄	N/A	515 nm visible light	<i>E. coli</i> 1337-H	2 log in 1h	16
g-C ₃ N ₄ /TiO ₂	0.6 g/L	300W Xe lamp with a 420 nm cutoff filter	<i>E. coli</i> K-12	7 log in 3 h	17
Ag/BiVO ₄	2 g/L	300W Xe lamp with a 420 nm cutoff filter	<i>E. coli</i>	7 log in 200 min	18
g-C ₃ N ₄ /rGO/α-S ₈	0.1 g/L	300W Xe lamp with a 400 nm cutoff filter	<i>E. coli</i> K-12	6.32 log in 4 h	19
AgVO ₃ QDs/g-C ₃ N ₄	0.75 g/L	300W Xe lamp with a 400 nm cutoff filter	<i>Salmonella</i> H9812	1.98 log in 10 min	20
Bi ₂ MoO ₆ /g-C ₃ N ₄	0.1 g/L	300W Xe lamp with a 420 nm cutoff filter	<i>E. coli</i> DH5α	6.0 log in 2.5 h	21
Ag ₂ WO ₄ /g-C ₃ N ₄	0.1 g/L	300W Xe lamp with a 420 nm cutoff filter	<i>E. coli</i>	7.0 log in 1.5 h	22
g-C ₃ N ₄ -AgBr	0.1 g/L	300W Xe lamp with a 400 nm cutoff filter	<i>E. coli</i>	6.0 log in 1h	23
BiVO ₄ /Ag/g-C ₃ N ₄	0.25 g/L	Eight 8W compacted fluorescent lamps	<i>E. coli</i> K-12	6.5 log in 1 h	This work

References

1. W. Wang, Y. Yu, T. An, G. Li, H. Y. Yip, J. C. Yu and P. K. Wong, Visible-light-driven photocatalytic inactivation of *E. coli* K-12 by bismuth vanadate nanotubes: bactericidal performance and mechanism, *Environ. Sci. Technol.*, 2012, **46**, 4599-4606.
2. D. Xia and I. M. Lo, Synthesis of magnetically separable Bi₂O₄/Fe₃O₄ hybrid nanocomposites with enhanced photocatalytic removal of ibuprofen under visible light irradiation, *Water Res.*, 2016, **100**, 393-404.
3. K.-I. Ishibashi, A. Fujishima, T. Watanabe and K. Hashimoto, Detection of active oxidative species in TiO₂ photocatalysis using the fluorescence technique, *Electrochem. Commun.*, 2000, **2**, 207-210.
4. T. W. Ng, L. Zhang, J. Liu, G. Huang, W. Wang and P. K. Wong, Visible-light-driven photocatalytic inactivation of *Escherichia coli* by magnetic Fe₂O₃-AgBr, *Water Res.*, 2016, **90**, 111-118.
5. S. Sun, W. Wang and L. Zhang, Bi₂WO₆ quantum dots decorated reduced graphene oxide: improved charge separation and enhanced photoconversion efficiency, *J. Phys. Chem. C*, 2013, **117**, 9113-9120.
6. R. Kern, R. Sastrawan, J. Ferber, R. Stangl and J. Luther, Modeling and interpretation of electrical impedance spectra of dye solar cells operated under open-circuit conditions, *Electrochim. Acta*, 2002, **47**, 4213-4225.
7. Y. Xu and M. A. Schoonen, The absolute energy positions of conduction and valence bands of selected semiconducting minerals, *Am. Mineral.*, 2000, **85**,

543-556.

8. M. Butler and D. Ginley, Prediction of flatband potentials at semiconductor-electrolyte interfaces from atomic electronegativities, *J. Electrochem. Soc.*, 1978, **125**, 228-232.
9. Y. Chen, X. Ma, D. Li, H. Wang and C. Huang, Mechanism of enhancing visible-light photocatalytic activity of BiVO₄ via hybridization of graphene based on a first-principles study, *RSC Adv.*, 2017, **7**, 4395-4401.
10. K. H. Leong, S. L. Liu, L. C. Sim, P. Saravanan, M. Jang and S. Ibrahim, Surface reconstruction of titania with g-C₃N₄ and Ag for promoting efficient electrons migration and enhanced visible light photocatalysis, *Appl. Surf. Sci.*, 2015, **358**, 370-376.
11. F. Chen, Q. Yang, Y. Wang, J. Zhao, D. Wang, X. Li, Z. Guo, H. Wang, Y. Deng and C. Niu, Novel ternary heterojunction photocatalyst of Ag nanoparticles and g-C₃N₄ nanosheets co-modified BiVO₄ for wider spectrum visible-light photocatalytic degradation of refractory pollutant, *Appl. Cat. B*, 2017, **205**, 133-147.
12. J. Huang, W. Ho and X. Wang, Metal-free disinfection effects induced by graphitic carbon nitride polymers under visible light illumination, *Chem. Commun.*, 2014, **50**, 4338-4340.
13. H. Zhao, H. Yu, X. Quan, S. Chen, Y. Zhang, H. Zhao and H. Wang, Fabrication of atomic single layer graphitic-C₃N₄ and its high performance of photocatalytic disinfection under visible light irradiation, *Appl. Cat. B*, , 2014,

- 152**, 46-50.
14. J. Xu, Z. Wang and Y. Zhu, Enhanced visible-light-driven photocatalytic disinfection performance and organic pollutant degradation activity of porous g-C₃N₄ nanosheets, *Acs Appl. Mater. Interfaces*, 2017, **9**, 27727-27735.
 15. S. Ma, S. Zhan, Y. Jia, Q. Shi and Q. Zhou, Enhanced disinfection application of Ag-modified g-C₃N₄ composite under visible light, *Appl. Cat. B.*, 2016, **186**, 77-87.
 16. M. J. Munoz-Batista, O. Fontelles-Carceller, M. Ferrer, M. Fernández-García and A. Kubacka, Disinfection capability of Ag/g-C₃N₄ composite photocatalysts under UV and visible light illumination, *Appl. Cat. B.*, 2016, **183**, 86-95.
 17. G. Li, X. Nie, J. Chen, Q. Jiang, T. An, P. K. Wong, H. Zhang, H. Zhao and H. Yamashita, Enhanced visible-light-driven photocatalytic inactivation of Escherichia coli using g-C₃N₄/TiO₂ hybrid photocatalyst synthesized using a hydrothermal-calcination approach, *Water Res.*, 2015, **86**, 17-24.
 18. A. Y. Booshehri, S. C.-K. Goh, J. Hong, R. Jiang and R. Xu, Effect of depositing silver nanoparticles on BiVO₄ in enhancing visible light photocatalytic inactivation of bacteria in water, *J. Mater. Chem. A*, 2014, **2**, 6209-6217.
 19. W. Wang, J. C. Yu, D. Xia, P. K. Wong and Y. Li, Graphene and g-C₃N₄ nanosheets cowrapped elemental α -sulfur as a novel metal-free heterojunction photocatalyst for bacterial inactivation under visible-light, *Environ. Sci.*

- Technol.*, 2013, **47**, 8724-8732.
20. R. Wang, X. Kong, W. Zhang, W. Zhu, L. Huang, J. Wang, X. Zhang, X. Liu, N. Hu and Y. Suo, Mechanism insight into rapid photocatalytic disinfection of Salmonella based on vanadate QDs-interspersed g-C₃N₄ heterostructures, *Appl. Catal.* 2018, **225**, 228-237.
 21. J. Li, Y. Yin, E. Liu, Y. Ma, J. Wan, J. Fan and X. Hu, In situ growing Bi₂MoO₆ on g-C₃N₄ nanosheets with enhanced photocatalytic hydrogen evolution and disinfection of bacteria under visible light irradiation, *J. Hazard. Mater.*, 2017, **321**, 183-192.
 22. Y. Li, Y. Li, S. Ma, P. Wang, Q. Hou, J. Han and S. Zhan, Efficient water disinfection with Ag₂WO₄-doped mesoporous g-C₃N₄ under visible light, *J. Hazard. Mater.*, 2017, **338**, 33-46.
 23. J. Deng, J. Liang, M. Li and M. Tong, Enhanced visible-light-driven photocatalytic bacteria disinfection by g-C₃N₄-AgBr, *Colloids Surf. B*, 2017, **152**, 49-57.